Dielectric functions and fundamental band gaps of $Cu_2In_4Se_7$, $CuGa_3Se_5$ and $CuGa_5Se_8$ crystals

2007 J. Phys. D: Appl. Phys. 40 740

(http://iopscience.iop.org/0022-3727/40/3/008)

INSTITUTE OF PHYSICS PUBLISHING JOURNAL OF PHYSICS D: APPLIED PHYSICS
J. Phys. D: Appl. Phys. **40** (2007) 740–748 doi:10.1088/0022-3727/40/3/008

Dielectric functions and fundamental band gaps of $Cu_2In_4Se_7$, $CuGa_3Se_5$ and $CuGa_5Se_8$ crystals

M León[1,4], S Levcenko[2], A Nateprov[2], A Nicorici[2], J M Merino[1], R Serna[3] and E Arushanov[1,2]

[1] Universidad Autónoma de Madrid, Departamento Física Aplicada, C-XII, 28049 Madrid, Spain
[2] Institute of Applied Physics, Academy of Sciences of Moldova, Chisinau, MD 2028, Moldova
[3] Instituto de Optica C.S.I.C, Serrano 121, 28006 Madrid, Spain

E-mail: maximo.leon@uam.es

Received 11 July 2006, in final form 7 November 2006
Published 19 January 2007
Online at stacks.iop.org/JPhysD/40/740

Abstract
Room temperature pseudodielectric function spectra $\varepsilon(\omega) = \varepsilon_1(\omega) + i\varepsilon_2(\omega)$ of the ordered defects compounds $Cu_2In_4Se_7$, $CuGa_3Se_5$ and $CuGa_5Se_8$ have been measured by spectroscopic ellipsometry. The values of refractive index n and extinction coefficient k are given. The structures observed in $\varepsilon(\omega)$ spectra have been analysed using different methods, including fitting the numerically differentiated experimental spectrum (second derivative) to analytical line shapes. As a result, the energies corresponding to the fundamental gap (E_0) and higher critical points have been determined. A linear correlation of the fundamental gap values with Ga/Cu atomic ratio contents in $CuGa_xSe_y$ samples is deduced.

1. Introduction

$CuInSe_2$ and related chalcopyrite-type semiconductors are leading candidates for absorbers in high-efficiency heterojunction solar cells. Devices based on $CuIn_{1-x}Ga_xSe_2$ have demonstrated efficiencies up to 19.3% [1]. Recent studies have shown the existence of an In-rich n-type material surface layer of $Cu(In_{1-x}Ga_x)_3Se_5$ on the absorber in some high-efficiency thin films cells. This layer, identified as an ordered defects compound (ODC) is expected to play an important role in the performance of the high-efficiency $CuIn_{1-x}Ga_xSe_2$-based solar cells [2, 3]. In a recent report of surface properties of $CuGaSe_2$ thin films, evidence of band gap widening [4] together with deviations from stoichiometry pointing to formation of ODC-related phases were also shown [5]. Therefore, a detailed study of the physical properties of these ODCs is essential. However, so far the characteristics of ODC have not yet been well determined. Some optical measurements were carried out on $Cu_2In_4Se_7$(I247), $CuGa_3Se_5$ (G35) and $CuGa_5Se_8$(G58) thin films and bulk samples and values of the fundamental band gap E_g were estimated [6–15].

Spectroscopic ellipsometry (SE) is an excellent technique for investigating the optical response of semiconductors, in particular, for determining the complex dielectric function $\varepsilon(\omega) = \varepsilon_1(\omega) + i\varepsilon_2(\omega)$. Accurate knowledge of the dielectric function over a wide range of wavelengths is indispensable for many applications [16]. It should also be mentioned that this function is related to the electronic band structure and can be used as a powerful source of experimental information on the latter [17].

In this work, the room temperature pseudodielectric function spectra of six samples, whose composition is around the three ODC, $Cu_2In_4Se_7$, $CuGa_3Se_5$ and $CuGa_5Se_8$, have been measured by SE. The energies corresponding to different electronic transitions have been determined.

2. Experimental methods

$Cu_2In_4Se_7$, $CuGa_3Se_5$ and $CuGa_5Se_8$ crystals belonging to the family of ordered defects compounds have been grown

[4] Author to whom any correspondence should be addressed.

Table 1. Data on compositional measurements of the studied samples carried out by energy dispersive x-ray microanalysis (EDAX).

Samples[a]	Cu, at.%	In(orGa), at.%	Se, at.%	In/Cu(or Ga/Cu)	Se/Cu
$Cu_2In_4Se_7$ (I247/B)	16.6	31.1	52.3	1.9	3.1
$CuGa_3Se_5$(G35T/B)	13.1	34.55	52.35	2.6	4.0
$CuGa_3Se_5$(G35B/B)	12.7	35.08	52.22	2.8	4.1
$CuGa_5Se_8$(G58T/B)	6.29	39.6	54.11	6.3	8.6
$CuGa_5Se_8$(G58B/B)	8.73	37.05	54.22	4.2	6.2
$CuGa_5Se_8$(G58/SC)	6.37	39.31	54.32	6.2	8.5

[a] T and B indicate that the sample studied was cut from the middle part of ingot closer to its top (T) or bottom (B) part. This explains some difference in composition between T/B and B/B samples. Variation of composition along the ingot was also observed in CuIn3Se5 as-grown ingot [27].
[b] B and SC indicate the methods (Bridgman and solid crystallization technique) used to grow ODC.

by the Bridgman method (B) and/or by the solid phase crystallization technique (SC). Compositional measurements were carried out by energy dispersive x-ray microanalysis (EDAX). The results of such analysis have been included in table 1. It is interesting to note that, in some cases, there are important deviations from the nominal stoichiometry, being specially remarkable for the nominal $CuGa_5Se_8$ samples, for which compositions from $CuGa_{4.2}Se_{6.2}$ to $CuGa_{6.3}Se_{8.6}$ have been obtained. This opens up the opportunity to study the optical properties as a function of the composition. The structural analysis was performed by x-ray measurements. The ingots of I247, G35 and G58 were polycrystalline single phase, with tetragonal structures. The samples were cut with plane-parallel faces, and polished with alumina powder. It is well known that the most serious problem in accurate determination of optical properties by SE is caused by deviation of the real sample surfaces from the ideal uncontaminated interfaces between measured materials and the ambient medium [17]. That is the reason for special attention being paid to the preparation of a good quality 'pure' surface. Surface organic impurities were eliminated using trichloroethylene, acetone, and ethanol in an ultrasonic bath, and finally the samples were blown dry with nitrogen. Immediately before performing the ellipsometry measurements the samples were chemically polished with a colloidal suspension (Buehler Mastermet) to eliminate oxide layers on the surface, rinsed in ethanol (5 min), and blown dry with nitrogen [18].

The complex dielectric functions, $\epsilon(\omega) = \epsilon_1(\omega) + i\epsilon_2(\omega)$, of the ODC samples have been measured by SE at room temperature in the photon energy range from 0.8 to 4.4 eV. The optical measurements were performed with a commercial ellipsometer (variable-angle spectroscopic ellipsometer J A Woollam) with a rotating polarizer. The ellipsometric spectra were measured at angles of incidence of 55° and 65° to ensure a consistent and accurate determination of the dielectric constant of the material [18]. The effects of a surface oxide layer have been diminished as previously explained, and the results can be assumed to be representative of the bulk material. Thus the two phase model (atmosphere sample) can be used to analyse the ellipsometry spectra and determine the dielectric function [19].

3. Results

Figures 1(*a*) and (*b*) show the experimental spectra of the imaginary $\varepsilon_2(\omega)$ and real $\varepsilon_1(\omega)$ components of the complex

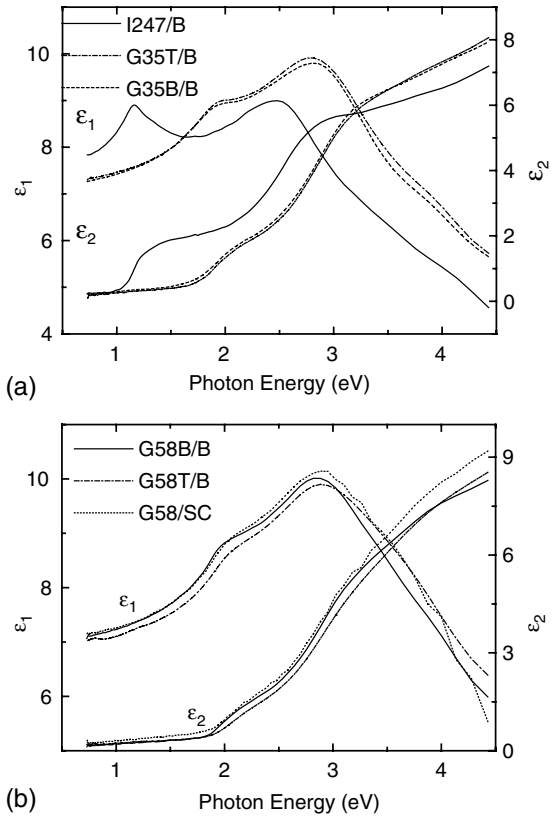

Figure 1. Real (ε_1) and imaginary (ε_2) part of the dielectric function versus energy for (*a*) $Cu_2In_4Se_7$ (I247/B) and $CuGa_3Se_5$ (G35T/B) crystals; (*b*) $CuGa_5Se_8$ (G58B/B, G58T/B and G58/SC) crystals.

dielectric function $\varepsilon(\omega)$ of I247/B, G35T/B, G35B/B and G58T/B, G58B/B, G58/SC samples, respectively. For convenience, numerical values of the refractive index n and extinction coefficient k are listed in table 2 for all studied samples. The real and imaginary refraction index n and k are the fundamental properties. However, a device physicist, who wants to assess the influence of the chalcopyrite optical properties on the solar cell device properties, would prefer to know the optical absorption coefficient α. The spectral dependence of $\alpha(\lambda) = (4\pi/\lambda)k(\lambda)$, where λ is the wavelength of light in the vacuum, is presented in figure 2(*a*) for $Cu_2In_4Se_7$, $CuGa_3Se_5$ and $CuGa_3Se_5$ crystals.

Table 2. Values of the real refraction index n and the extinction coefficient k.

	I35/B		G35B/B		G35T/B		G58T/B		G58B/B		G58/SC	
E (eV)	n	k	n	k	n	k	n	k	n	k	n	k
0.8	2.811	0.045	2.703	0.041	2.710	0.035	2.661	0.038	2.670	0.029	2.678	0.045
0.9	2.840	0.049	2.713	0.047	2.722	0.041	2.657	0.038	2.678	0.033	2.687	0.051
1.0	2.886	0.058	2.725	0.053	2.732	0.047	2.666	0.043	2.689	0.039	2.695	0.057
1.1	2.955	0.098	2.739	0.060	2.745	0.052	2.680	0.046	2.701	0.044	2.707	0.062
1.2	2.980	0.210	2.755	0.063	2.759	0.058	2.695	0.051	2.717	0.046	2.719	0.066
1.3	2.945	0.266	2.774	0.067	2.777	0.061	2.707	0.053	2.733	0.050	2.736	0.071
1.4	2.919	0.303	2.796	0.071	2.798	0.065	2.723	0.055	2.752	0.051	2.755	0.076
1.5	2.897	0.324	2.825	0.080	2.825	0.070	2.743	0.060	2.775	0.057	2.777	0.082
1.6	2.885	0.336	2.862	0.092	2.859	0.078	2.767	0.062	2.804	0.059	2.803	0.086
1.7	2.886	0.347	2.902	0.109	2.901	0.092	2.796	0.067	2.836	0.065	2.834	0.092
1.8	2.890	0.356	2.945	0.139	2.949	0.120	2.833	0.073	2.877	0.073	2.874	0.103
1.9	2.911	0.370	2.984	0.186	2.991	0.170	2.878	0.088	2.934	0.101	2.922	0.122
2.0	2.931	0.390	3.000	0.240	3.009	0.221	2.925	0.119	2.974	0.152	2.969	0.161
2.1	2.953	0.416	3.009	0.280	3.018	0.264	2.958	0.161	2.996	0.198	3.002	0.207
2.2	2.992	0.451	3.024	0.313	3.033	0.297	2.984	0.200	3.015	0.235	3.027	0.247
2.3	3.023	0.503	3.046	0.341	3.053	0.326	3.008	0.235	3.036	0.269	3.052	0.285
2.3	3.023	0.503	3.046	0.341	3.053	0.326	3.008	0.235	3.036	0.269	3.052	0.285
2.4	3.049	0.565	3.073	0.377	3.082	0.360	3.036	0.269	3.063	0.301	3.081	0.321
2.5	3.067	0.639	3.104	0.421	3.115	0.402	3.069	0.307	3.096	0.339	3.116	0.361
2.6	3.064	0.731	3.137	0.477	3.151	0.454	3.106	0.353	3.133	0.389	3.153	0.410
2.7	3.034	0.818	3.168	0.543	3.184	0.523	3.143	0.408	3.173	0.448	3.189	0.472
2.8	2.990	0.885	3.192	0.622	3.205	0.604	3.174	0.476	3.204	0.521	3.219	0.545
2.9	2.946	0.934	3.203	0.711	3.210	0.692	3.193	0.551	3.219	0.605	3.237	0.624
3.0	2.901	0.971	3.191	0.800	3.199	0.780	3.199	0.630	3.218	0.692	3.241	0.704
3.1	2.859	0.999	3.160	0.884	3.172	0.859	3.195	0.706	3.202	0.772	3.234	0.781
3.2	2.829	1.013	3.117	0.950	3.130	0.925	3.183	0.776	3.174	0.841	3.219	0.851
3.3	2.798	1.040	3.067	1.003	3.086	0.982	3.167	0.842	3.146	0.904	3.200	0.917
3.4	2.769	1.069	3.018	1.048	3.045	1.030	3.149	0.906	3.119	0.963	3.180	0.982
3.5	2.749	1.094	2.976	1.088	3.009	1.074	3.131	0.969	3.090	1.019	3.159	1.046
3.6	2.719	1.122	2.944	1.125	2.979	1.116	3.112	1.032	3.061	1.075	3.138	1.110
3.7	2.693	1.154	2.920	1.160	2.954	1.156	3.091	1.093	3.035	1.132	3.114	1.173
3.8	2.675	1.185	2.900	1.195	2.933	1.194	3.068	1.153	3.011	1.186	3.086	1.235
3.9	2.656	1.208	2.879	1.232	2.911	1.232	3.041	1.210	2.988	1.237	3.053	1.297
4.0	2.635	1.236	2.857	1.271	2.887	1.270	3.012	1.265	2.961	1.283	3.017	1.357
4.1	2.619	1.266	2.832	1.310	2.858	1.309	2.984	1.315	2.927	1.326	2.981	1.415
4.2	2.606	1.305	2.809	1.348	2.832	1.350	2.959	1.363	2.896	1.367	2.949	1.471
4.3	2.589	1.349	2.790	1.385	2.810	1.391	2.938	1.408	2.869	1.407	2.921	1.525
4.4	2.556	1.395	2.778	1.420	2.798	1.431	2.924	1.450	2.852	1.445	2.902	1.574

The n values in the transparency region of the studied samples decrease when increasing the wavelength λ (table 2). The refractive index versus λ can be fitted using a simple Cauchy dispersion relation with two coefficients, n_0 and C. The first coefficient (n_0) can be found fitting the data to the equation $n = n_0 + (C/\lambda^2)$ or by plotting $[1/(n^2 - 1)$ versus $(1/\lambda^2)]$ (figure 2(*b*)) [20]. In the latter case, the values of n_0 are determined as the intercept at $(1/\lambda^2) = 0$. Both methods gave the same n_0 values of about 2.69, 2.67 and 2.62 for $Cu_2In_4Se_7$, $CuGa_3Se_5$ and $CuGa_5Se_8$, respectively. Our data on n are close to those reported for $CuInSe_2$ and $CuGaSe_2$ [21, 22]. The Cauchy dispersion accurately fits the experimental values of I247/B, G35T/B and G58B/B for λ higher than 1000 nm and 800 nm, respectively (figure 2(*b*)).

3.1. Theoretical models

The structures observed in the $\varepsilon(\omega)$ spectra are attributed to interband critical points (CPs), related to regions of the band structure with large or singular point electronic density of states. The structure can be analysed in terms of standard analytic line shapes [17]

$$\varepsilon(\omega) = C - A\mathrm{e}^{\mathrm{i}\varphi}(\omega - E + \mathrm{i}\gamma)^m, \qquad (1)$$

where A is the critical-point parameters amplitude, E is the energy threshold, γ is the broadening and φ is the phase angle. In order to enhance the structure present in the $\varepsilon(\omega)$ spectra and to obtain the CP parameters, the second derivative spectra of the complex dielectric function, $\mathrm{d}^2\varepsilon(\omega)/\mathrm{d}\omega^2$, from our ε data was numerically calculated with the standard technique of smoothing polynomials. Parameters A, E, γ and φ are determined by fitting the numerically obtained second derivative spectra of the experimental $\varepsilon(\omega)$ to equation (1). The exponent m equals to $-1/2$ and $1/2$ for one- (1D) and three-dimensional (3D) CPs, respectively. In the case of two-dimensional (2D) CPs, m= 0 and then $\varepsilon(\omega) = C - A\mathrm{e}^{\mathrm{i}\varphi}\ln(\omega - E + \mathrm{i}\gamma)$. Discrete excitons with a Lorentzian line shape (0D) are represented by $m = -1$. From the fact that CPs are directly related to regions of large or singular joint electronic density of states, direct information on the energy separation of valence and conduction bands (interband gaps) can be obtained, which can be compared with band-structure calculations [17].

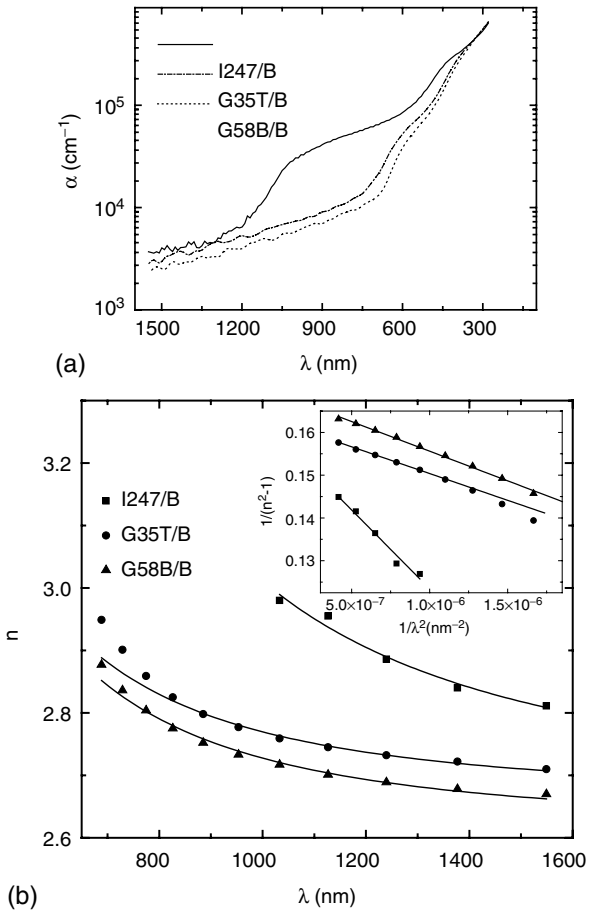

Figure 2. (*a*) Spectral dependence of the absorption coefficient α for $Cu_2In_4Se_7$ (I247/B), $CuGa_3Se_5$ (G35T/B) and $CuGa_5Se_8$ (G58B/B) crystals; (*b*) n versus λ for $Cu_2In_4Se_7$ (I247/B), $CuGa_3Se_5$ (G35T/B) and $CuGa_5Se_8$ (G58B/B) crystals. The solid lines are a fit to $n = n_0 + (C/\lambda_2)$. The inset displays $1/(n^2-1)$ versus $1/\lambda^2$ dependence.

The second-derivative of the complex dielectric function (SD) can be written as [18]:

for $m \neq 0$:

$$\frac{\mathrm{d}^2\varepsilon}{\mathrm{d}\omega^2} = A'(\Omega)^{(m-2)/2}\left\{\cos\left[(m-2)\arccos\left(\frac{\omega-E}{\Omega^{1/2}}\right)+\varphi\right] + \mathrm{i}\sin\left[(m-2)\arccos\left(\frac{\omega-E}{\Omega^{1/2}}\right)+\varphi\right]\right\}$$

with $A' = -m(m-1)A, \quad \Omega = (\omega-E)^2+\gamma^2,$ and (2*a*)

for $m = 0$:

$$\frac{\mathrm{d}^2\varepsilon}{\mathrm{d}\omega^2} = \frac{A}{\Omega}\left\{\cos\left[-2\arccos\left(\frac{\omega-E}{\Omega^{1/2}}\right)+\varphi\right] + \mathrm{i}\sin\left[-2\arccos\left(\frac{\omega-E}{\Omega^{1/2}}\right)+\varphi\right]\right\}. \quad (2b)$$

This method (we name it as SDM) was successfully applied to different semiconducting materials to identify and evaluate the energy of the electronic transitions [17, 18, 20] However, SDM has five fitting parameters, which could be decreased using the module of the first derivative of $\varepsilon(\omega)$. Such a module can be written as

$$\left|\frac{\mathrm{d}\varepsilon}{\mathrm{d}\omega}\right|^2 = \frac{\mathrm{d}\varepsilon_1}{\mathrm{d}\omega}^2 + \frac{\mathrm{d}\varepsilon_2}{\mathrm{d}\omega}^2, \quad (3)$$

which for $m \neq 0$ is

$$\left|\frac{\mathrm{d}\varepsilon}{\mathrm{d}\omega}\right|^2 = A^2m^2\left((\omega-E)^2+\gamma^2\right)^{(m-1)}, \quad (3a)$$

and for $m = 0$ is

$$\left|\frac{\mathrm{d}\varepsilon}{\mathrm{d}\omega}\right|^2 = \frac{A^2}{(\omega-E)^2+\gamma^2}. \quad (3b)$$

The latter method (named MM in the paper) has four fitting parameters.

Recently, Kawashima *et al* [16] have successfully used a simplified model for interband transitions to analyse the SE data of $CuGaSe_2$ and $CuInSe_2$ where the $E_{0\alpha}$ ($\alpha = A, B,$ and C) gaps in chalcopyrite crystals may be assigned to the 3D M_0 critical point. Assuming that the valence and conduction bands are parabolic and using the Kramers–Kronig transformation, the contribution of these gaps to $\varepsilon(\omega)$ can be written as [16]

$$\varepsilon(E) = \sum_{\alpha=A,B,C} A_{0\alpha}E_{0\alpha}^{-3/2}f(\chi_{0\alpha}) \quad (4)$$

with $A_{0\alpha} = \frac{4}{3}(3/\mu_{0\alpha})^{3/2}P_{0\alpha}^2$, $f(\chi_{0\alpha}) = \chi_{0\alpha}^{-2}\left[2-(1+\chi_{0\alpha})^{1/2}-(1-\chi_{0\alpha})^{1/2}\right]$, $\chi_{0\alpha} = (E+i\Gamma)/E_{0\alpha}$, where $\mu_{0\alpha}$ is the combined density-of-states mass, $P_{0\alpha}^2$ is the squared momentum-matrix element, and Γ is the damping energy of the $E_{0\alpha}$ gap.

The fundamental optical spectra of our ODC (figure 1) as well as $CuGaSe_2$ and $CuInSe_2$ reveal CPs at energies higher than the lowest direct gaps ($E_{0\alpha}$) which may correspond to transitions at points N, T, etc in the Brillouin zone (BZ). Assuming that these CPs can be considered as damped harmonic oscillators (DHOs)

$$\varepsilon(E) = \frac{C_n}{(1-\chi_n^2)-\mathrm{i}\chi_n\gamma_n} \quad (5)$$

with $\chi_n = E/E_n$, where C_n and γ_n are, respectively, the strength and non-dimensional broadening parameters of the nth DHO and E_n is the energy value of the CP. Note that the DHO is a different representation of a 2D M_1 CP both with and without the existence of the excitonic interaction [16].

On the basis of equations (4) and (5) and the Adachi model [16], expressions for both the second derivative and the module of the first derivative have been determined (see equations (4*a*) and (4*b*) and (5*a*)–(5*d*) in the appendix) and applied to our experimental data as a second derivative chalcopyrite method (SDCM) and a module chalcopyrite method (MCM). In both cases, the number of fitting parameters is equal to 3, lower than that used in the cases of SDM and MM. It is worth mentioning that one should normally calculate the separate contributions from $E_{0\alpha}$ ($\alpha = A, B,$ and C) critical points according to equation (4), but in our case splitting among these critical points is not observed and hence $E_{0\alpha}$ has been treated as a single degenerate one.

Table 3. Fit parameters of the CPs for the samples studied.

Transitions	Parameters	SDM	MM	Parameters	SDCM	MCM
Sample I247/B						
$E_0(\Gamma_4-\Gamma_1)$	E(eV)	1.150(5)	1.140(5)	$E_{0\alpha}$(eV)	1.133(2)	1.120(5)
	γ(eV)	0.103(6)	1.135(5)	Γ(eV)	0.048(7)	0.044(3)
E_1(A)	E(eV)	2.60(2)	2.60(1)	$E_{1\beta}$(eV)	2.56(1)	2.52(1)
$N_1(V_1)-N_1(C_1)$	γ(eV)	0.30(2)	0.26(1)	$\Gamma_{1\beta}$(eV)	0.33(2)	0.29(1)
Sample G35T/B						
$E_0(\Gamma_4-\Gamma_1)$	E(eV)	1.88(1)	1.860(5)	$E_{0\alpha}$(eV)	1.855(6)	1.78(1)
	γ(eV)	0.26(2)	0.30(1)	Γ(eV)	0.11(1)	0.13(1)
E_1(A)	E(eV)	2.86(2)	2.94(1)	$E_{1\beta}$(eV)	2.91(1)	2.830(5)
$N_1(V_1)-N_1(C_1)$	γ(eV)	0.37(2)	0.37(1)	$\Gamma_{1\beta}$(eV)	0.36(2)	0.39(1)
E_1(B)	E(eV)	3.94(7)	4.12(3)	E_n(eV)	4.15(15)	4.3(1)
$N_1(V_2)-N_1(C_1)$	γ(eV)	0.21(4)	0.56(4)	γ	0.26(12)	0.45(8)
Sample G35B/B						
$E_0(\Gamma_4-\Gamma_1)$	E(eV)	1.90(2)	1.86(1)	$E_{0\alpha}$(eV)	1.86(1)	1.77(2)
	γ(eV)	0.26(2)	0.34(2)	Γ(eV)	0.13(2)	0.15(2)
E_1(A)	E(eV)	2.95(2)	2.96(1)	$E_{1\beta}$(eV)	2.91(1)	2.850(5)
$N_1(V_1)-N_1(C_1)$	γ(eV)	0.34(2)	0.37(1)	$\Gamma_{1\beta}$(eV)	0.36(2)	0.39(1)
E_1(B)	E(eV)	3.9(1)	4.03(1)	E_n(eV)	4.05(6)	4.10(3)
$N_1(V_2)-N_1(C_1)$	γ(eV)	0.2(1)	0.44(3)	γ	0.10(5)	0.36(3)
Sample G58T/B						
$E_0(\Gamma_4-\Gamma_1)$	E(eV)	1.94(2)		$E_{0\alpha}$(eV)	1.99(1)	
	γ(eV)	0.29(2)		Γ(eV)	0.12(2)	
E_1(A)	E(eV)	2.80(2)		$E_{1\beta}$(eV)	2.94(2)	
$N_1(V_1)-N_1(C_1)$	γ(eV)	0.38(2)		$\Gamma_{1\beta}$(eV)	0.39(4)	
E_1(B)	E(eV)	3.96(14)		E_n(eV)	3.99(5)	
$N_1(V_2)-N_1(C_1)$	γ(eV)	0.46(11)		γ	0.37(8)	
Sample G58B/B						
$E_0(\Gamma_4-\Gamma_1)$	E(eV)	1.90(1)		$E_{0\alpha}$(eV)	1.92(1)	
	γ(eV)	0.22(1)		Γ(eV)	0.10(1)	
E_1(A)	E(eV)	2.85(3)		$E_{1\beta}$(eV)	2.91(2)	
$N_1(V_1)-N_1(C_1)$	γ(eV)	0.34(3)		$\Gamma_{1\beta}$(eV)	0.33(4)	
E_1(B)	E(eV)	4.1(2)		E_n(eV)	4.0(1)	
$N_1(V_2)-N_1(C_1)$	γ(eV)	0.25(11)		γ	0.33(13)	
Sample G58/SC						
$E_0(\Gamma_4-\Gamma_1)$	E(eV)	1.93(5)		$E_{0\alpha}$(eV)	1.97(1)	
	γ(eV)	0.29(1)		Γ(eV)	0.12(2)	
E_1(A)	E(eV)	2.85(3)		$E_{1\beta}$(eV)	2.91(2)	
$N_1(V_1)-N_1(C_1)$	γ(eV)	0.37(2)		$\Gamma_{1\beta}$(eV)	0.38(4)	
E_1(B)	E(eV)	4.0(2)		E_n(eV)	3.92(7)	
$N_1(V_2)-N_1(C_1)$	γ(eV)	0.35(15)		γ	0.29(9)	

4. Discussion

The experimental spectra of the imaginary $\varepsilon_2(\omega)$ and real ε_1 (ω) components of the complex dielectric function $\varepsilon(\omega)$ of I247/B, G35T/B, G35B/B and G58T/B, G58B/B, G58/SC samples (figure 1(*a*) and (*b*)) show peaks that correspond to CPs of energy transitions of the electronic band structure. In the region below 2 eV, the fundamental energy gap $E_0 = E_g$ is well distinguished for each sample, and in the region below 4.4 eV a second $E_1(A)$ and a third energy threshold $E_1(B)$ can be observed. The precise values of the E_g and E_1 energy thresholds have been determined by theoretical fitting of both the second derivative and the module of the first derivative, using the 4 models mentioned in the previous paragraph, namely SDM, MM, SDCM and MCM. The sets of two mainly obtained fitting parameters for the methods used are compiled in table 3 for all the studied samples. The different values given to the exponent m, used as a fixed parameter in SDM and MM, are detailed further.

In figures 3(*a*)–5(*a*) and 3(*b*)–5(*b*), the second derivative with respect to the photon energy of the experimental real and imaginary components of the dielectric function, $\mathrm{d}^2\varepsilon_2/\mathrm{d}\omega^2$ and $\mathrm{d}^2\varepsilon_1/\mathrm{d}\omega^2$, and the module of the first derivative are, respectively, plotted. The theoretical fittings according to SDM and MM for samples I247/B, G35T/B (figures 3 and 4), and SDCM and MCM for samples G58T/B and G58B/B (figure 5) are also shown. These fittings have been obtained considering CPs of three types: 0D (discrete exciton) in the E_g region for SDM and MM, with $m = -1$; 3D in the E_g region for SDCM and SCM, and 2D in the E_1 region for all models, with $m = 0$. It is worth mentioning that all applied models show reasonable agreement between the experimental data and the calculated curves. SDM and SDCM are widely used and suitable for the chalcopyrite structure materials. MM and MCM models have not been used earlier. Both methods are especially useful to apply if the numerical derivation is inaccurate, introducing numeral noise, etc.

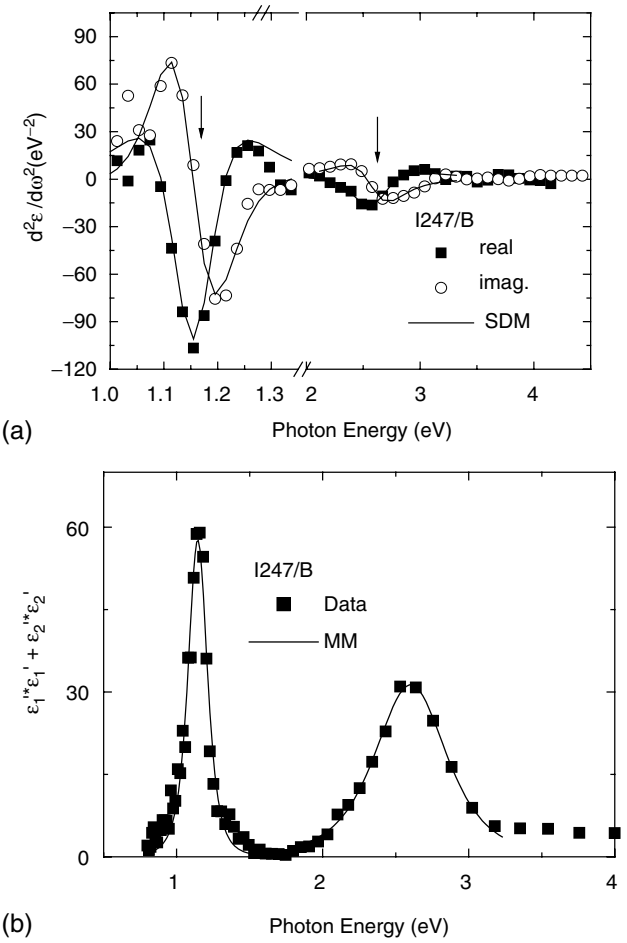

Figure 3. (*a*) Second numeral derivative spectra of the real (ε_1) and imaginary (ε_2) part of the dielectric function for $Cu_2In_4Se_7$ (I247/B) and the theoretical fitting using the SDM method; (*b*) Module of the first derivative spectra for $Cu_2In_4Se_7$ (I247/B) and the theoretical fitting using the MM method.

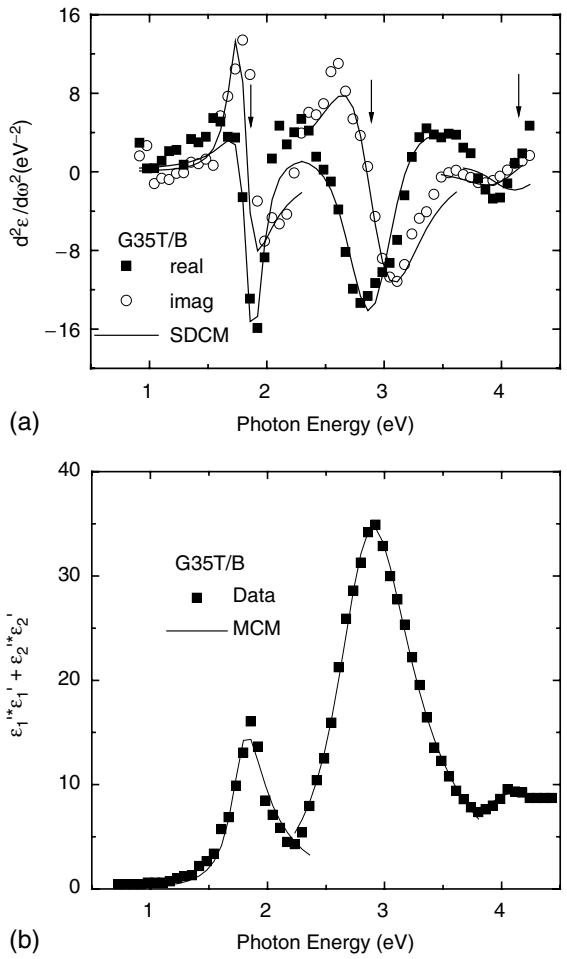

Figure 4. (*a*) Second numeral derivative spectra of the real (ε_1) and imaginary (ε_2) part of the dielectric function for $CuGa_3Se_5$ (G35T/B) and the theoretical fitting using SDCM method; (*b*) Module of the first derivative spectra for $CuGa_3Se_5$ (G35T/B) and the theoretical fitting using the MCM method.

The values of the interband CP parameters (strength, threshold energy, broadening and phase angle) have been derived from the applied models. It is worth mentioning that both the fundamental energy gap value, E_g, and the broadening factor, γ_n, increase (figures 6(*a*) and (*b*) as the gallium concentration increases (table 1). Averaged values of E_g determined using E_0 data estimated on the bases of different models (see table 3) have been used to plot E_g versus Ga/Cu dependence (figure 6(*b*)). The linear correlation of the fundamental gap values with the Ga/Cu atomic ratio contents allows the prediction of the E_g value by just measuring the composition. The second result indicates that the characteristic structures of the dielectric function of $CuGa_3Se_5$and $CuGa_5Se_8$ crystals slowly vanish as the concentration of gallium increases. A similar effect has been observed in $CuInSe_2$ and GaAs [24]. Following [24], we assume that the lattice structure of our ODC is damaged by the higher defect concentration induced by the off-stoichiometry.

Band-structure calculations needed to perform identifications of the energy transitions observed are not available for our compounds but well known for $CuInSe_2$ and $CuGaSe_2$. Since the latter are similar to our studied ODC, identifications of the observed energy transitions have been made considering the CIS and CGS band-structure calculations. As has been established for these compounds, the main transitions contributing to $\varepsilon(\omega)$ occur at the Brillouin zone (BZ) centre (fundamental gap at Γ) and BZ edge points N and T (predominant upper transitions) [21, 22].

The energy threshold of the fundamental absorption edge $E_0 = E_g$ is well identified in the spectrum of both the second numerical derivative and module of the first derivative, and can be related to an electronic transition of Γ type. This threshold corresponds to a direct transition from the valence band maximum to the conduction band minimum, i.e. the E_g value. Our data about the room temperature values of E_g in the studied materials (1.12–1.16; 1.78–1.87 and 1.92–1.97 eV for I247, G35 and G58, respectively, table 3) are in reasonable agreement with those (0.99–1.22 [6, 7, 9, 11], 1.81–1.86 [10, 13, 25] and 1.85 eV [14, 25]) determined using optical data. The variation in the reported values of the ODC band gap can be attributed to compositional changes. Some contribution could be also due to strain effects (especially in the case of thin films) or temperature differences. When compared with other semiconductor compounds, the chalcopyrites and ODCs exhibit an unusually high tolerance to stoichiometric

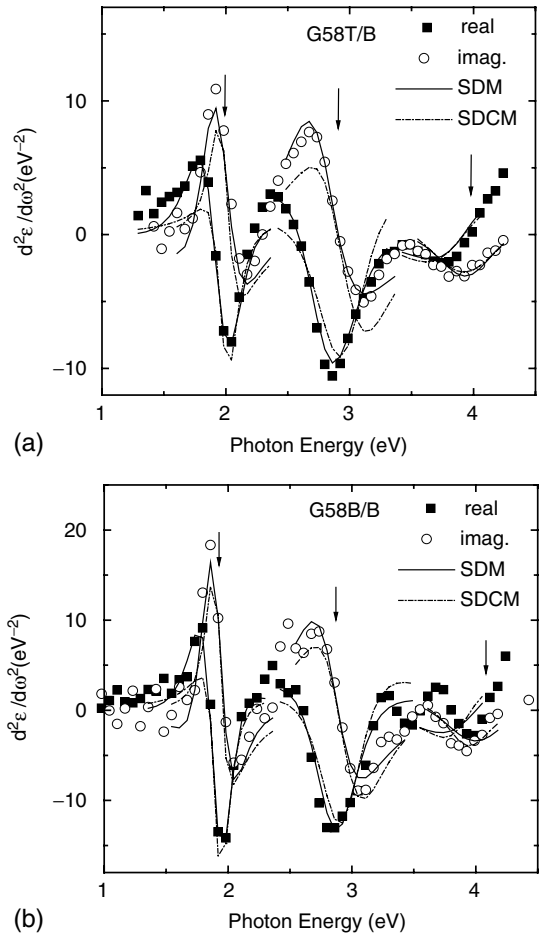

Figure 5. Second numeral derivative spectra of the real (ε_1) and imaginary (ε_2) part of the dielectric function and the theoretical fitting using the SDM and SDCM methods for (*a*) $CuGa_5Se_8$ (G58T/B) and (*b*) $CuGa_5Se_8$ (G58B/B).

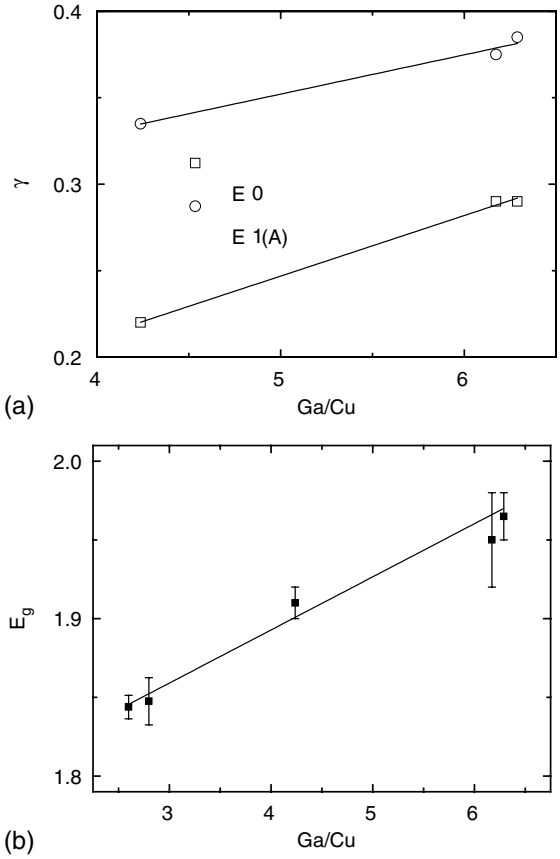

Figure 6. (*a*) Ga/Cu dependence of the broadening parameters γ of critical points E_0, E_1(A) and E_1(B) for $CuGa_5Se_8$ crystals. The line shows linear fits to the data, calculated using SDM. (*b*) Ga/Cu dependence of the fundamental energy gap.

deviations. In fact, $CuInSe_2$ shows band gap values ranging from 0.94 to 1.04 eV. Our $CuGa_5Se_8$ samples show different E_g values (table 3) increasing with Se/Cu and Ga/Cu ratios (figure 6), and similar behaviour has been observed in the $CuIn_3Se_5$ and $CuIn_5Se_8$ samples [9, 26]. In the region of 2.5–4.4 eV, one transition for I35/B and two transitions for the remaining samples, named as E_1(A) and E_1(B), have been observed. We assume that they can be related to N-type transitions following [21, 22], where ellipsometric data of $CuInSe_2$ and $CuGaSe_2$ were analysed. The measured energy separation between these two transitions corresponds to the crystal-field splitting of the valence band at the N point. In the studied materials, the distance between $N_{1v}^{(1)}$ and $N_{1v}^{(2)}$ is about 1–1.1 eV and a close value (0.8 eV) was reported for the $CuInSe_2$ and $CuGaSe_2$ crystals [21, 22].

5. Conclusions

SE has been used to determine room temperature pseudodielectric function spectra of CuInSe and CuGaSe crystal compounds grown by the Bridgman method and/or the solid phase crystallisation technique. The measured $\varepsilon(\omega)$ spectra reveal structures at the lowest direct gap (E_0) and higher energy CPs. The structures observed have been analysed using four different methods (SDM, MM, SDCM, and MCM). All models used permit to get good enough fitting to our experimental data on $\varepsilon(\omega)$ within the accuracy of the measurement. The values of the interband CP parameters (strength, threshold energy, broadening and phase angle) have been derived from the applied models. The analysis of the dielectric function has allowed us to identify and evaluate the energy of the electronic transitions E_0, $E_1(A)$ and $E_1(B)$. The present results offer a valuable set of data for CuInSe and CuGaSe compounds with stoichiometry close to $CuIn_2Se_3$, $CuGa_3Se_4$ and $CuGa_5Se_8$. We also show that there is a dependence of the optical properties on the composition, specially a linear correlation of the fundamental gap values with the Ga/Cu atomic ratio, and thus it is found that the data of this work can be useful for the design of solar cells based on ODC.

Acknowledgments

Financial support from the INTAS Program (Project 03-51-6314) Comunidad de Madrid (Project FOTOFLEX S-0505/ENE/0123) and from the Spanish Government MEC projects ENE 2004-07446-C02-01/ALT/ and MAT2003-01490 is acknowledged. The authors would also like to acknowledge the technical support provided by A Ripa during the ellipsometry measurements. One of the authors (SL) would

like to thank the World Federation of Scientists for financial support.

Appendix

Module (MCM) from ε'$(\omega)$of the 3D M_0 CP can be written as below presented in equation (4*a*):

$$\begin{aligned}
&\mathrm{Mod}[\varepsilon(E)] = A_{0\alpha}^2(\Gamma^2{+}E^2)^3\big\{(9\Gamma^2 + (4E_{0\alpha} - 3E)^2)T_1 \\
&-2(T_1T_3)^{1/2}\big\{(-16E_{0\alpha}^2 + 9(\Gamma^2 + E^2))\cos((T_4 - T_2)/2) \\
&+8(E_{0\alpha}T_1)^{1/2}\big[(4E_{0\alpha} - 3E)\cos(T_4/2) - 3\Gamma\sin(T_4/2)\big] \\
&+24E_{0\alpha}\Gamma\sin((T_4 - T_2)/2)\big\} + T_3\big\{9\Gamma^2 + (4E_{0\alpha} + 3E)^2 \\
&+64E_{0\alpha}T_1 + 16(E_{0\alpha}T_1)^{1/2}\big[-(4E_{0\alpha} + 3E)\cos(T_2/2) \\
&-3\Gamma\sin(T_2/2)\big]\big\}\big\}/(4T_3T_1T_5^{12}),
\end{aligned}$$

with

$$\begin{aligned}
&T_1 = [(E_{0\alpha} + E)^2 + \Gamma^2]^{1/2},\ T_2 = \mathrm{acos}((E_{0\alpha} + E)/T_1), \\
&T_3 = [(E_{0\alpha} - E)^2 + \Gamma^2]^{1/2},\ T_4 = -\mathrm{acos}((E_{0\alpha} - E)/T_3), \\
&T_5 = (E^2 + \Gamma^2)^{1/2}.
\end{aligned}$$

The second derivative (SDCM) from $\varepsilon(\omega)$ of the 3D M_0 CP can be written as below presented in equation (4*b*):

$$\begin{aligned}
&\frac{\mathrm{d}^2\varepsilon_2(E)}{\mathrm{d}E^2} = -A_{0\alpha}\big\{-8(E_{0\alpha}T_3)^{3/2}T_5^2T_1[\Gamma(\Gamma^2 - 3E^2)\cos(T_2/2) \\
&-E(-3\Gamma^2 + E^2)\sin(T_2/2))] + 24(E_{0\alpha}T_3)^{3/2}T_1^2 \\
&\times[4\Gamma E(\Gamma^2 - E^2)\cos(T_2/2) + (\Gamma^4{-}6\Gamma^2E^2{+}E^4)\sin(T_2/2)] \\
&+(E_{0\alpha}T_3)^{3/2}T_5^4\big[2\Gamma E\cos(3T_2/2) + (-\Gamma^2 + E^2)\sin(3T_2/2)\big] \\
&+T_1^{3/2}\big\{-192E_{0\alpha}^2\Gamma E(\Gamma^2{-}E^2)T_3^{3/2} + 8E_{0\alpha}T_5^2T_3[\Gamma(\Gamma^2{-}3E^2) \\
&\times\cos(T_4/2) - E(-3\Gamma^2 + E^2)\sin(T_4/2)] + 24E_{0\alpha}^2T_3^2 \\
&\times[4\Gamma E(\Gamma^2 - E^2)\cos(T_4/2) + (\Gamma^4{-}6\Gamma^2E^2{+}E^4)\sin(T_4/2)] \\
&+T_5^4\big[2\Gamma E\cos(3T_4/2) + (-\Gamma^2{+}E^2)\sin(3T_4/2)\big]\big\}\big\}/ \\
&(4(E_{0\alpha}T_1T_3)^{3/2}T_5^8),
\end{aligned}$$

$$\begin{aligned}
&\frac{\mathrm{d}^2\varepsilon_1(E)}{dE^2} = -A_{0\alpha}\big\{-8(E_{0\alpha}T_3)^{3/2}T_5^2T_1 \\
&\times\big[(-3\Gamma^2E + E^3)\cos(T_2/2) + \Gamma(\Gamma^2{-}3E^2)\sin(T_2/2)\big] \\
&+24(E_{0\alpha}T_3)^{3/2}T_1^2\big[(\Gamma^4{-}6\Gamma^2E^2{+}E^4)\cos(T_2/2) + 4\Gamma E \\
&(-\Gamma^2{+}E^2)\sin(T_2/2)\big]{+}(E_{0\alpha}T_3)^{3/2}T_5^4[(\Gamma^2{-}E^2)\cos(3T_2/2) \\
&+2\Gamma E\sin(3T_2/2)]{+}T_1^{3/2}\big\{-48E_{0\alpha}^2(\Gamma^4{-}6\Gamma^2E^2{+}E^4)T_3^{3/2} \\
&+8E_{0\alpha}T_5^2T_3[(-3\Gamma^2E + E^3)\cos(T_4/2) + \Gamma(\Gamma^2{-}3E^2) \\
&\times\sin(T_4/2)] + 24(E_{0\alpha}T_3)^2\big[(\Gamma^4{-}6\Gamma^2E^2{+}E^4)\cos(T_4/2) \\
&+4\Gamma E(-\Gamma^2 + E^2)\sin(T_4/2)\big]{+}T_5^4[(\Gamma^2 - E^2)\cos(3T_4/2) \\
&+2\Gamma E\sin(3T_4\big\}/2)]\big\}/(4(E_{0\alpha}T_1T_3)^{3/2}T_5^8),
\end{aligned}$$

with

$$\begin{aligned}
&T_1{=}\big[(E_{0\alpha}{+}E)^2{+}\Gamma^2\big]^{1/2}, \qquad T_2{=}\ \mathrm{acos}((E_{0\alpha}{+}E)/T_1), \\
&T_3{=}\big[(1 - E/E_{0\alpha})^2{+}(\Gamma/E_{0\alpha})^2\big]^{1/2}, \\
&T_4{=}\ -\mathrm{acos}((1 - E/E_{0\alpha})/T_3), \\
&T_5{=}\ (E^2{+}\Gamma^2)^{1/2}.
\end{aligned}$$

Module (MCM) from $\varepsilon^{'}(\omega)$ of damped harmonic oscillators (DHOs) can be written as below presented in equation (5*a*):

$$\mathrm{Mod}\,[\varepsilon(E)] = C^2E_n^4(4E^2{+}\gamma^2E_n^2)/((E^2{-}E_n^2)^2{+}(E_n\gamma E)^2)^2.$$

The second derivative (SDCM) from $\varepsilon(\omega)$ of DHOs can be written as below presented equation (5*b*):

$$\begin{aligned}
\frac{\mathrm{d}^2\varepsilon_2(E)}{\mathrm{d}E^2} &= 2CE_n^3\gamma E\{E_n^6(4 - 3\gamma^2) + E_n^4\gamma^2(-6{+}\gamma^2)E^2 \\
&\quad +E_n^2(-12 + 5\gamma^2)E^4{+}8E^6{+}2(E_n^2 - E^2)T_1^2\}/T_1^6, \\
\frac{\mathrm{d}^2\varepsilon_1(E)}{\mathrm{d}E^2} &= 2CE_n^2\{-E_n^8\gamma^2{+}E_n^6(4 - 9\gamma^2{+}3\gamma^4)E^2 \\
&\quad +E_n^4(-12 + 9\gamma^2{+}\gamma^4)E^4{+}E_n^2(12{+}\gamma^2)E^6 - 4E^8 \\
&\quad +\big[E_n^4{-}E_n^2(2{+}\gamma^2)E^2{+}E^4\big]T_1^2\}/T_1^6,
\end{aligned}$$

where

$$T_1{=}\big[(E_n^2{-}E^2)^2{+}(E_n\gamma E)^2\big]^{1/2}.$$

The modified Adachi model

$$\varepsilon(E) = -B_{1\beta}\chi_{1\beta}^{-2}\mathrm{Ln}(1 - \chi_{1\beta}^2),$$

where

$$\chi_{1\beta} = (E + \mathrm{i}\Gamma_{1\beta})/E_{1\beta},$$

and $B_{1\beta}$ and $\Gamma_{1\beta}$ are the strengths and damping constants of the $E_{1\beta}$ transitions, respectively.

Module (MCM) from $\varepsilon'(\omega)$ of the Adachi model can be written as below presented equation (5*c*):

$$\begin{aligned}
\mathrm{Mod}\,[\varepsilon(E)] &= 4B_{1\beta}^2(\Gamma_{1\beta}^2 + E^2)^3\big\{(\Gamma_{1\beta}^2 + (E_{1\beta} - E)^2) \\
&\quad\times(\Gamma_{1\beta}^2 + E^2)^2(\Gamma_{1\beta}^2 + (E_{1\beta}{+}E)^2) + 2E_{1\beta}^4T_1^2\big[2E_{1\beta}^2\Gamma_{1\beta}ET_3 \\
&\quad -\big(E_{1\beta}^2(\Gamma_{1\beta}^2 - E^2) + (\Gamma_{1\beta}^2 + E^2)^2\big)\ln T_1\big] \\
&\quad +E_{1\beta}^8T_1^4(T_3^2 + 2\ln T_1)\big\}/(E_{1\beta}^4T_1^4T_2^{12})
\end{aligned}$$

with

$$\begin{aligned}
&T_1{=}\big[\big(1 + (\Gamma_{1\beta}^2{-}E^2)/E_{1\beta}^2\big)^2{+}4\Gamma_{1\beta}^2E^2/(E_{1\beta}^4)\big]^{1/2}, \\
&T_2{=}\ (\Gamma_{1\beta}^2{+}E^2)^{1/2}, \\
&T_3{=}\ -\mathrm{acos}\big(\big(1 + (\Gamma_{1\beta}^2{-}E^2)/E_{1\beta}^2\big)/T_1\big).
\end{aligned}$$

Second derivative (SDCM) from $\varepsilon(\omega)$ of Adachi model can be written as below presented equation (5*d*):

$$\begin{aligned}
&\frac{\mathrm{d}^2\varepsilon_2}{\mathrm{d}E^2} = -2B_{1\beta}\big\{-2\Gamma_{1\beta}E[4(E_{1\beta}^2 + \Gamma_{1\beta}^2 - E^2)(\Gamma_{1\beta}^2 + E^2)^2 \\
&+3E_{1\beta}^4(E_{1\beta}^2 + 2\Gamma_{1\beta}^2{-}2E^2)T_1^2]T_2^4{+}3E_{1\beta}^8T_1^4\big[(\Gamma_{1\beta}^4{-}6\Gamma_{1\beta}^2E^2 \\
&+E^4)T_3{+}4\Gamma_{1\beta}E(\Gamma_{1\beta}^2{-}E^2)\ln T_1\big]\big\}/(E_{1\beta}^6T_1^4T_2^8), \\
&\frac{\mathrm{d}^2\varepsilon_1}{\mathrm{d}E^2} = -2B_{1\beta}\big\{-\big[2(\Gamma_{1\beta}^2 + E^2)^2(E_{1\beta}^4 + \Gamma_{1\beta}^4 - 6\Gamma_{1\beta}^2E^2{+}E^4 \\
&+2E_{1\beta}^2(\Gamma_{1\beta}^2{-}E^2)) + 3E_{1\beta}^4(\Gamma_{1\beta}^4{-}6\Gamma_{1\beta}^2E^2 + E^4 \\
&+E_{1\beta}^2(\Gamma_{1\beta}^2 - E^2))T_1^2\big]T_2^4{+}3E_{1\beta}^8T_1^4[(-4\Gamma_{1\beta}^3E + 4\Gamma_{1\beta}E^3)T_3 \\
&+(\Gamma_{1\beta}^4{-}6\Gamma_{1\beta}^2E^2{+}E^4)\ln T_1]\big\}/(E_{1\beta}^6T_1^4T_2^8),
\end{aligned}$$

where

$$\begin{aligned}
&T_1{=}[(1 + (\Gamma_{1\beta}^2{-}E^2)/E_{1\beta}^2)^2{+}4\Gamma_{1\beta}^2E^2/E_{1\beta}^4]^{1/2}, \\
&T_2{=}\ (\Gamma_{1\beta}^2{+}E^2)^{1/2}, \quad T_3{=}\ -\mathrm{acos}\left(\left(1 + (\Gamma_{1\beta}^2{-}E^2)/E_{1\beta}^2\right)/T_1\right).
\end{aligned}$$

References

[1] Ramanathan K, Teeter G, Keane J and Noufi R 2005 *Thin Solid Films* **480–481** 499

[2] Kessler J, Schmid D, Schafler R, Schock H W and MenezesS 1993 *Proc. 23rd IEEE Photovoltaic Conference (Louisville)* (New York: IEEE) p 549

[3] Xiao H Z, Yang Chung L and Rockett A 1994 *J. Appl. Phys.* **76** 1503

[4] Meeder A, Weinhardt L, Stresing R, Fuertes Marrón D, Würz R, Babu S M, Schedel-Niedrig Th, Lux-Steiner M Ch, Heske S and Umbach E 2003 *J. Phys. Chem. Solids* **64** 1553

[5] Würz R, Rusu M, Schedel-Niedrig Th, Lux-Steiner M Ch, Blum H, Hävecker M, Kleimenov E, Knop-Gericke A and Schlogl R 2005 *Surf. Science* **580** 80
Lehmann S *et al* 2006 *Thin Solid Films* **511–512** 623

[6] Reddy Y B K and Raja V S 2004 *Mater. Lett.* **58** 1839

[7] Rincon C, Wasim S M, Marin G and Sanchez Perez G 2003 *J. Appl. Phys.* **93** 8939

[8] Negami T, Kohara N, Nishitani M, Wada T and Hirao T 1995 *Appl. Phys. Lett.* **67** 825

[9] Mahanty S, Merino J M, Diaz R, Rueda F, Martin de Vidales J L and Leon M 1998 *Inst. Phys. Conf. Ser.* **152** 499

[10] Marin G, Rincon C, Wasim S M, Sanches Perez G and Molina I 1999 *J. Alloys Compounds* **283** 1

[11] Shirakata S, Chichubu S, Miyake H, Isomura S, Nakanishi H and Sugiyama K 1998 *Inst. Phys. Conf. Ser.* **152** 598

[12] Wasim S M, Marin G, Rincon C, Bocaranda P and Sanchez Perez G 2000 *J. Phys. Chem. Sol.* **61** 669

[13] Rincon C, Wasim S M, Marin G and Molina I 2003 *J. Appl. Phys.* **93** 780

[14] Marin G, Wasim S M, Rincon C, Sanches Perez G, Bocaranda P, Molina I, Guevara R and Delgado J M 2004 *J. Appl. Phys.* **95** 8280
Duran L, Guerrero C, Hernandes E, Delgado J M, Contreras J, Wasim S M and Durante Rincon C A 2003 *J. Phys. Chem. Solids* **64** 1907

[15] Orlova N S, Bodnar I V and Kushner T L 2003 *J. Phys.Chem. Sol.* **64** 1895

[16] Kawashima T, Adachi S, Miyake H and Sugiyama K 1998 *J. Appl. Phys.* **84** 5202

[17] Lautenschlager P, Garriga M, Logothetidis S and Cardona M 1987 *Phys. Rev.* B **35** 9174
Cardona M 1969 *Modulation Spectroscopy* (New York: Academic)

[18] Albornoz J G, Serna R and Leon M 2005 *J. Appl. Phys.* **97** 103515

[19] Topkins H G and McGahan W A 1999 *Spectroscopic Ellipsometry and Reflectometry* (New York: Wiley)

[20] Moss T S, Burrel G J and Ellis B 1973 *Semiconductor Opto-Electronics* (London: Butterworths)
Swanepoel R 1983 *J. Phys. E. Sci. Instrum.* **16** 1214

[21] Alonso M I, Garrida M, Durante Rincon C A and Leon M 2000 *J. Appl. Phys.* **88** 5796

[22] Alonso M I, Wakita K, Pascual J, Garriga M and Yamamoto N 2001 *Phys. Rev.* B **63** 075203

[23] Djurisic A B and Herbert Li E 1999 *J. Appl. Phys.* **85** 2848

[24] Zeaiter K, Yanuar A and Llinares C 2001 *Solar Energy Mater. Solar Cells* **70** 213

[25] Wasim S M, Rincon C, Marin G and Delgado J M 2000 *Appl. Phys. Lett.* **77** 94

[26] Marin G, Wasim S M, Rincon C, Sanchez Perez G, Power Ch and Mora A E 1998 *J. Appl. Phys.* **83** 3364

[27] Wang H P, Shih I and Champness C H 2000 *Thin Solid Films* **361–362** 494